Mon. Not. R. Astron. Soc. **398,** 1573–1581 (2009) doi:10.1111/j.1365-2966.2009.15224.x

# Investigating the far-IR/radio correlation of star-forming Galaxies to $z = 3$

N. Seymour,[1,2]★ M. Huynh,[3] T. Dwelly,[4] M. Symeonidis,[1] A. Hopkins,[5] I. M. McHardy,[4] M. J. Page[1] and G. Rieke[6]

[1]*Mullard Space Science Laboratory, UCL, Holmbury St Mary, Dorking, Surrey RH5 6NT*
[2]*Spitzer Science Center, Caltech, 1200 East California Boulevard, Pasadena, CA 91125, USA*
[3]*Infrared Processingand Analysis Center, MS220-6, California Institute of Technology, Pasadena, CA 91125, USA*
[4]*School of Physics & Astronomy, University of Southampton, Highfield, Southampton SO17 1BJ*
[5]*Anglo-Australian Observatory, PO Box 296 Epping, NSW 1710, Australia*
[6]*Steward Observatory, Tucson, AZ 85721, USA*

Accepted 2009 June 9. Received 2009 June 8; in original form 2008 December 23



**ABSTRACT**

In order to examine the far-infrared (far-IR)/radio correlation at high redshift, we have studied the *Spitzer* 70 μm/far-IR properties of sub-mJy radio sources from the 13[H] *XMM–Newton/Chandra* Deep Field by redshift and galaxy type: active galactic nucleus (AGN) or star-forming galaxy (SFG). We directly detect 70 μm counterparts (at $>3\sigma$ significance) for 22.5 per cent (92/408) of the radio sources, while for the rest we perform stacking analysis by redshift and galaxy type. For the sources detected at 70 μm, we find that the median and scatter of the observed flux density ratio, $q_{70}$, are similar to previous results in the literature, but with a slight decrease in $q_{70}$ towards higher redshifts. Of the radio sources detected at 70 μm 8/92 were already classified as AGN, but two of which maybe SFGs. For the stacked sources, we obtain a detection for the SFGs at every redshift bin which implies they have mean flux densities a factor ∼5 below the original 70 μm detection limit. For the stacked AGN, we obtain a detection only in our highest redshift bin ($1 \leq z \leq 5$) where we may be sampling hot dust associated with the AGN at rest frame 12−35 μm. The combined observed mean value of $q_{70}$ for the SFGs (detected and non-detected at 70 μm) decreases gradually with redshift, consistent with tracks derived from empirical spectral energy distributions (SEDs) of local SFGs. Upon closer inspection and when comparing with tracks of appropriate luminosity, the values of $q_{70}$ broadly agree at low redshift. However, at $z \sim 1$, the observed $q_{70}$ [for ultra-luminous infrared galaxies (ULIRGs)] is $2\,\sigma$ below the value seen for local ULIRGs tracks, implying a difference in the SED between local and $z \sim 1$ ULIRGs. At higher redshifts, the convergence of the tracks and the higher uncertainties in $q_{70}$ do not allow us to determine if such a difference persists.

**Key words:** galaxies: evolution – starburst – infrared: galaxies – radio continuum: galaxies.

## 1 INTRODUCTION

The tight correlation over many orders of magnitude between the far-infrared (far-IR) and radio luminosity of star-forming galaxies (SFGs) has been well studied in the local Universe (e.g. Helou, Soifer & Rowan-Robinson 1985; Condon et al. 1991; Yun, Reddy & Condon 2001). The radio emission of normal galaxies is dominated by synchrotron radiation from relativistic electrons and free–free emission from H II regions (Condon 1992). Both of these mechanisms are related to the presence of young, massive ($M > 8\,M_{\odot}$) stars; radio non-thermal emission arises from electrons accelerated by supernovae from these stars and thermal emission from ionized H II regions. The mid- and far-IR emission arises from dust absorption and subsequent reradiation of UV/optical light. Deviations from this correlation are seen within galaxies (Hughes et al. 2006; Murphy et al. 2006), but these probably derive from the longer mean free path of the relativistic electrons compared to the dust heating UV photons, and the scatter in the relation within local galaxies is similar to that seen between local galaxies (e.g. Yun et al. 2001). Some authors (Hughes et al. 2006; Murphy et al. 2006) have suggested that the far-IR/radio correlation may also have some dependence on star formation rate (SFR) and SFR density within a galaxy.

The far-IR/radio correlation is important as it is used to define the radio luminosity/SFR relation (e.g. Bell 2003) and can also

★E-mail: nps@mssl.ucl.ac.uk

allow the selection of radio-loud active galactic nuclei (AGN) (e.g. Donley et al. 2005). Hence, determining whether this relation deviates significantly or becomes less tight at higher redshifts and higher luminosities is of great consequence. In particular, the interpretation of data from the next generation of radio surveys, which will find Milky-Way-like SFGs out to high redshifts, will rely on the application of the radio luminosity/SFR relation. In the distant Universe, the relation between the mid-IR and radio luminosities has been shown to approximately hold to $z \sim 1$ (Garrett 2002; Appleton et al. 2004) based on *Infrared Space Observatory* (*ISO*) and *Spitzer* observations, although there are some disagreements about the proportionality constant. At $z \geq 1$ using millimetre and submillimetre observations Kovács et al. (2006) and Vlahakis, Eales & Dunne (2007) find evidence of a decrease of $\sim$0.2 dex in the far-IR/radio ratio compared to the local value, but it was shown in Seymour et al. (2008, hereafter S08) that the relation does approximately hold by comparing AGN-free distant and local samples of powerful starbursts at the same rest-frame far-IR wavelengths. However, the S08 study was small consisting of 11 sources at $1.5 \geq z \geq 3$.

Several different mechanisms could lead to departures from the radio/far-IR correlation at high redshift. Deviations at low luminosities have been noted (Bell 2003), but these occur in low-SFR sources (SFR $\leq 3\,\mathrm{M}_{\odot}\,\mathrm{yr}^{-1}$) which cannot be detected to any great distance in current radio surveys. Modelling of the radio/far-IR relation in dusty starbursts has shown that the correlation is a natural result in any starburst if synchrotron emission dominates inverse Compton, and the electron cooling time is shorter than the analogous fading time of the supernovae rate (Bressan, Silva & Granato 2002). However, deviations may be possible in both the early phase of a starburst, when the radio thermal component dominates the non-thermal component, and in the post-starburst phase, when the bulk of the non-thermal component originates from less massive stars. Other potential mechanisms that could lead to deviations from the relation include: (i) evolution in metallicity and dust properties, with accompanying changes in the far-IR spectral energy distributions (SEDs); (ii) evolution in magnetic field properties; (iii) quenching from the cosmic microwave background; or (iv) the effects of hot intracluster gas in dense environments (e.g. Miller & Owen 2001).

The most sensitive IR probe of high-redshift star formation with current facilities is the 24 μm band of the Multiband Imaging Photometer for Spitzer (MIPS) instrument (Rieke et al. 2004) on board the *Spitzer Space Telescope* (Werner et al. 2004). The cross-correlation of radio and 24 μm data from many deep surveys has led to several evaluations of a mid-IR/radio relation (Boyle et al. 2007; Beswick et al. 2008; Ibar et al. 2008; Garn & Alexander 2009). Some of these authors (Boyle et al. 2007; Beswick et al. 2008) observe a change in the mid-IR/radio ratio at faint radio and/or 24 μm flux densities, but as these authors discuss there are different populations being analysed depending on the selection of the parent population. Also, studies using 24 μm observations suffer from the shift of this band with redshift to shorter wavelengths where it no longer tracks the cool dust directly associated with star formation and into a regime where features due to polycyclic aromatic hydrocarbons (PAHs) may dominate. Furthermore, it is possible that different processes (star formation or AGN) dominate in each of the radio and 24 μm bands.

We aim to overcome some of these difficulties by using a sample of sub-mJy radio sources that have been categorized by the physical process that dominates their radio emission: star formation or AGN activity. In S08, we used several radio-related discriminators (radio morphology, radio spectral index, observed 24 μm/radio and $K$-band/radio flux density ratios) to separate these two populations in a very deep 1.4 GHz survey and confirmed the expected result (from modelling of the radio source counts; Rowan-Robinson et al. 1991; Hopkins 2004) that the SFG population dominates at the faintest radio flux densities, $S_{1.4\,\mathrm{GHz}} \leq 0.1$ mJy, but with a significant, $\sim \frac{1}{3}$, contribution from AGN.

In this paper, we examine the far-IR/radio correlation of the sub-mJy radio population by galaxy type and redshift by studying their 70 μm emission. Studying the emission at 70 μm has several advantages over that at 24 μm. This far-IR band is more comparable to the IR wavelengths used in the early studies of this correlation (i.e. using the *IRAS* 60 and 100 μm bands; Helou et al. 1985). The 70 μm band also samples the SED of local ultraluminous infrared galaxies (ULIRGs) closer to its peak (60 μm $\leq \lambda_{\mathrm{rest}} \leq$ 120 μm) than the 24 μm band and is a more direct measure of the total IR luminosity and hence SFR. Furthermore, given the redshift range of the sample examined here, an analysis at 24 μm would probe rest-frame wavelengths 7 μm $\leq \lambda_{\mathrm{rest}} \leq$ 24 μm, well away from the cold dust related to the ongoing star formation, and into a regime containing uncertain tracers of star formation (e.g. PAHs) as well as complications due to silicate absorption/emission features and possible AGN contamination of unknown strength. The 70 μm band has a few disadvantages: its relative shallowness compared to equivalent surveys at 24 μm and the potential confusion at faint flux densities due to the low resolution at 70 μm. We can overcome the first of these issues through the use of stacking techniques on sources not detected at 70 μm. The latter problem is mostly overcome by the accurate (subarcsec) positions of our radio sources, the parent population we are investigating.

We have chosen to adopt in this paper a similar philosophy to that used in S08, where we make no assumptions about the SED of the sources we observe, but use *observed* flux density ratios as a function of redshift at all times, and then compare these to models. This approach is the most appropriate since at each redshift slice we are looking at sources with different luminosities which may not be directly comparable to each other. We present our data analysis and cross-correlation in Section 2, and in Section 3 we present the results of our cross-correlation and stacking analysis. We discuss our results in Section 4 and present our conclusions in Section 5. Throughout we use a concordance model of Universe expansion, $\Omega_M = 1 - \Omega_\Lambda = 0.3$, $\Omega_0 = 1$ and $H_0 = 70\,\mathrm{km\,s^{-1}\,Mpc^{-1}}$ (Spergel et al. 2003).

## 2 DATA ANALYSIS

### 2.1 Radio data and separation by galaxy type

The radio sample used in this work was originally presented in Seymour, McHardy & Gunn (2004, hereafter S04) which described our deep Very Large Array (VLA) 1.4 GHz observations of the 13$^{\mathrm{H}}$ *XMM/Chandra* Deep Survey Field (M$^{\mathrm{c}}$Hardy et al. 1998). We obtained a rms noise of 7.5 μJy at the centre of the single VLA pointing and found 449 sources at 4$\sigma$ significance out to a diameter of 30 arcmin. Over the last decade, we have obtained deep follow-up optical, near-IR and *Spitzer* imaging. We have obtained spectra for 163/449 radio sources and these spectra were used to calibrate our 14-band optical/near-/mid-IR photometric redshifts for the radio sources (see Dwelly et al. in preparation, for a summary). Our spectroscopy revealed one radio source to be a star which we remove from further consideration. Only sources that were detected in at least four bands (236 sources) have photometric redshifts. Hence, our parent sample consists of 448 radio sources

of which 162 have spectroscopic redshifts, 236 have photometric redshifts and 50 sources have unknown redshifts.

In S08, we described the separation of our parent sample into galaxy type: AGN and SFG. In that paper, we made the assumption that one of these processes dominated the radio emission and that we could use diagnostics directly related to the radio emission to separate these radio sources. These empirical diagnostics were radio morphology (from combined Multi-Element Radio Linked Interferometer (MERLIN)/VLA observations), radio spectral index (from combined VLA 1.4/4.8 GHz data), and two observed flux density ratios plotted as function of redshift: 24 μm/radio and radio/$K$-band. Our analysis in S08 found 269/449 faint 1.4 GHz sources to be SFGs and the remainder to be AGN.

Our radio catalogue is not complete to the 30 μJy detection limit due to radio instrumental effects. The attenuation of the primary beam of the VLA away from the pointing centre is by far the strongest effect and causes a decrease in the sensitivity of the survey by a factor of ∼2 at the edge of the field of view. In S04, we calculated correction factors due to this effect (as well as other more minor ones) and used these correction factors in determining the radio source counts; each source was given a weight corresponding to its detection plus a factor representing all the sources at the same flux density, but not detected due to the effective decrease in the sky area at faint flux densities. These correction factors were also used in determining the comoving SFR density history in S08 and we use these same factors again here. These factors only apply to sources below 100 μJy and are generally low, ≤2 for 50 μJy $< S_{1.4\,\mathrm{GHz}} <$ 100 μJy, but do reach values ≥2 at $S_{1.4\,\mathrm{GHz}} < 50$ μJy. We discuss the impact of the use of these correction factors in Section 3.5.

### 2.2 *Spitzer* MIPS 70 μm data

The MIPS observations of the 13$^{\mathrm{H}}$ field consist of a deep scan map using all three bands (24, 70 and 160 μm) which covers approximately 0.5 × 1 deg$^2$. These observations were obtained in 2005 July as part of MIPS instrument team guaranteed time observations (GTO) time (PI G. Rieke, programme identification number 81). Our 1.4 GHz radio observations cover one end of this MIPS map. The 70 μm basic calibrated data (BCDs) from the Spitzer Science Center were processed offline using the Germanium Reprocessing Tools (GERT[1]), following the filtering techniques adopted for the extragalactic First Look Survey (xFLS; Frayer et al. 2006). In particular, negative sidelobes near bright sources were removed using a combination of high pass time median and column filtering with the bright sources masked. The BCDs were then mosaiced in the standard fashion with MOPEX[1] and the rms noise in the final 70 μm map was ∼2 mJy per beam. A list of sources was produced with the APEX[1] software, which performs robust point spread functon (PSF) fitting, down to 3$\sigma$ (6 mJy). Flux densities were divided by a factor of 0.918 to colour correct for a $\nu \times F_\nu =$ constant SED (the most appropriate for the sources we are detecting) as the MIPS absolute flux calibration references a 10$^4$ K blackbody. The source list is incomplete at the 3$\sigma$ level of significance and may not be free from spurious sources, but spurious sources are not a concern for our approach, where we simply intend to measure the 70 μm flux density of each member of our parent radio sample. We note that the probability of an individual 70 μm source being matched by chance with a radio source is low (≤1.5 per cent).

[1] Available from http://ssc.spitzer.caltech.edu/postbcd/

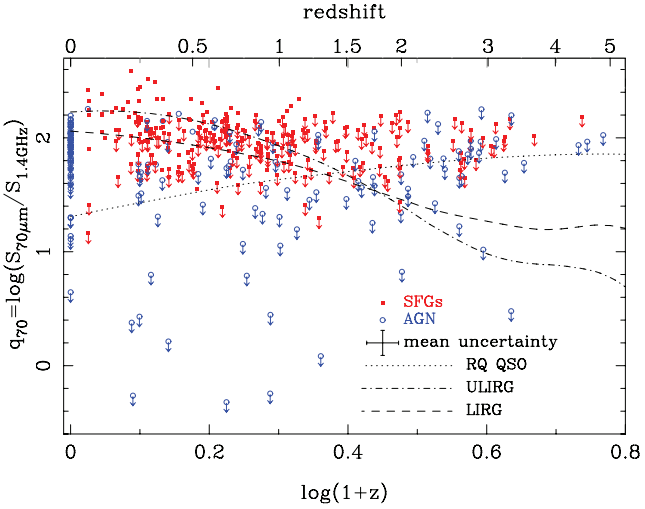


**Figure 1.** The *observed* far-IR/radio flux density ratio ($q_{70} = \log[S_{70\,\mu\mathrm{m}}/S_{1.4\,\mathrm{GHz}}]$) of our radio-selected population plotted as a function of redshift; sources with unknown redshifts are plotted at $z = 0$. Sources are separated by galaxy type (SFGs: red squares, AGN: blue open circles) and upper limits represent non-detections at 70 μm at a 3$\sigma$ limit of 6 mJy. Average individual uncertainties are indicated although we note the uncertainty in the redshift is considerably less for the $\sim \frac{1}{3}$ sources with spectroscopic redshifts. The tracks of local ultraluminous infrared galaxies, ULIRGs, (derived from empirical observations, Rieke et al. 2009) are shown as reference. The ULIRG [log ($L_{\mathrm{IR}}/\mathrm{L}_\odot$) ≥ 12] has a higher SFR than the LIRG [log ($L_{\mathrm{IR}}/\mathrm{L}_\odot$) ≥ 11] by a factor of 10 and has a higher observed value of $q_{70}$ until $z \sim 2.5$. We also show the track of a radio-quiet QSO from Elvis et al. (1994).

Out of the 448 radio sources in the parent sample, 40 were not covered by the 70 μm image. From the remaining 408 sources, we find 92 with 70 μm counterparts within 5 arcsec from our ≥3$\sigma$ catalogue. These radio sources with 70 μm counterparts all have redshifts and include eight AGN and 84 SFGs. Hence, there remain 316 radio sources with only 70 μm upper limits.

### 2.3 Stacking of 70 μm data

To push our analysis to fainter 70 μm flux densities, we made stacked postage stamp cutouts of the 70 μm image at the locations of radio sources that were not matched to sources in the 70 μm catalogue. Each cutout was 128 × 128 arcsec$^2$ (32 × 32 pixels after resampling to 4 arcsec pixels in the mosaicing) in size. These cutouts were combined using a weighted mean (where the weight is the inverse of the square of the local rms).

The stacking was done in several bins of galaxy type (SFG, AGN) and redshift. In S08, we found redshifts for all our SFGs so the sources with unknown redshifts comprise one bin at $z =$ 0 of 47 AGN which are too faint in the optical and near-IR for photometric redshifts to be determined (none of which are detected at 70 μm). The bins were initially chosen to be of equal size in log $(1 + z)$, except some bins were amalgamated to ensure each bin had at least 30 sources: the two highest redshift SFG bins were combined and the five AGN bins were combined into two. Such amalgamation is necessary in order to obtain a significant improvement, i.e. $\geq \sqrt{30}$, in the sensitivity compared to the unstacked image. Similar to Huynh et al. (2007), offset stacked images with the same number of sources per bin were generated by randomly choosing a nearby position (<64 arcsec or <3.5 FWHM) in the 70 μm image for each stacked source. 200 randomly offset stacks were generated, and the

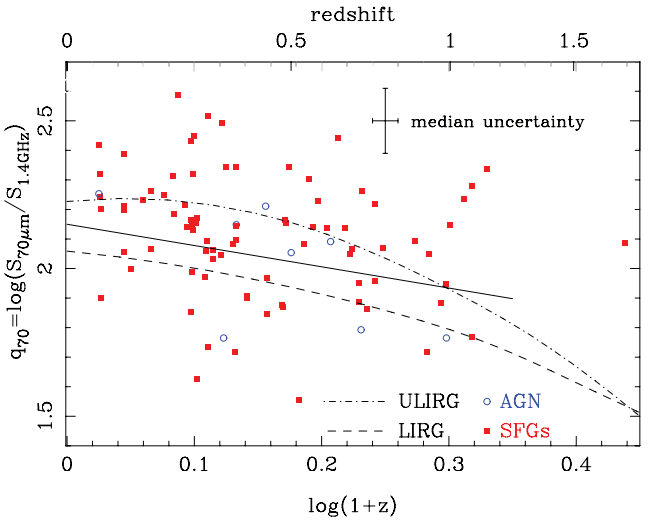


**Figure 2.** The observed $q_{70}$ as function of redshift for just the radio sources detected at 70 μm (SFGs: red squares, AGN: blue open circles). The solid line indicates the best-fitting linear regression to these data (SFGs and AGN). We discuss the 70 μm detection of eight AGN in the text.

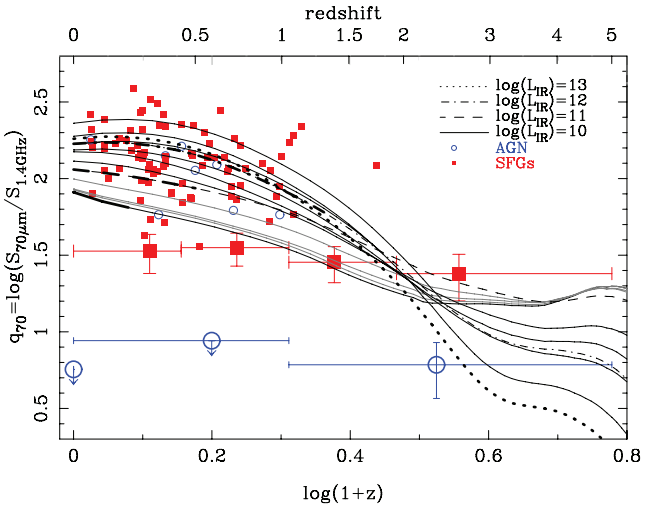


**Figure 3.** The observed value of $q_{70}$ plotted as a function of redshift and source type (SFGs: red squares, AGN: open blue circles) for 70 μm detected sources and stacked non-detections at 70 μm. Overlaid are star forming tracks covering a range of IR luminosities from Rieke et al. (2009) at luminosities indicated in the figure including those in Fig 1. These lines become thinner at the redshift, a template of a given luminosity becomes undetectable in our radio survey. The thin grey lines represent tracks from templates at intermediate luminosities with interval of 0.25 dex. The mean flux density ratios of sources undetected at 70 μm, derived from the stacked 70 μm flux densities, are indicated by larger symbols with error bars (indicating the width of the redshift bin and the uncertainty in $q_{70}$). The SFGs have a detected flux density in each redshift bin and hence a determinable value of $q_{70}$ whereas AGN are only detected in the highest redshift bin.

uncertainty in the stacked flux density is taken to be the standard deviation of these 200 measured values.

## 3 RESULTS

### 3.1 Observed $q_{70}$ for the whole sample

The IR/radio correlation (at mid- or far-IR wavelengths) is commonly defined as $q_{\rm IR} = \log[S_{\rm IR}/S_{1.4\,\rm GHz}]$ (e.g. Yun et al. 2001; Appleton et al. 2004; Beswick et al. 2008; Ibar et al. 2008). We examine our *observed* values of $q_{70}$ in Fig. 1 as a function of redshift for all sources (including upper limits for the radio sources not detected at 70 μm). Fig. 1 shows a wide scatter for the whole parent population, although most values are upper limits due to non-detection at 70 μm. The sources with very low $q_{70}$ upper limits, as seen for many of the AGN, are typically the brightest radio sources in our survey. As our radio survey is flux density limited, and hence suffers from some redshift/luminosity degeneracy, it is not appropriate to fit to $q_{70}$ as a function of redshift without accounting for the different luminosity ranges probed at each redshift. We choose to plot tracks calculated from templates of local galaxies, but shifted to the corresponding redshift and convolved with the appropriate band passes, as a direct comparison to our *observed* values of $q_{70}$. We overlay tracks derived from empirical local LIRG and ULIRG SEDs (Rieke et al. 2009) and an unobscured radio-quiet AGN SED (Elvis et al. 1994). The starburst templates are derived from the mean of many local galaxies of the appropriate luminosity. We note an empirical M82 track would lie marginally below the LIRG track presented here.

### 3.2 Observed $q_{70}$ for the detected sample

The radio sources detected at 70 μm all have values of $q_{70} > 1.5$ (Fig. 2) mainly due to the sensitivity limit of the 70 μm observations. We calculate the median value of $q_{70}$ for this subsample in order to compare with earlier work. We find a value of $q_{70} = 2.13 \pm 0.24$ (using a biweight estimator; Beers, Flynn & Gebhardt 1990), very similar to that found by (Appleton et al. 2004): $q_{70} = 2.16 \pm 0.17$ (covering a similar redshift range). Additionally, we derive values separately for each galaxy type obtaining a similar value for the 84 SFGs ($q_{70} = 2.13 \pm 0.24$) and a slightly lower value for the eight AGN ($q_{70} = 2.02 \pm 0.22$). While SFG and AGN results are marginally statistically different, the similarity in values is probably due to the depth of the 70 μm data not being able to detect sources, regardless of type, with a low value of $q_{70}$. Naturally, the values of observed median $q_{70}$ for SFG and AGN are only upper limits for the radio selected sample as a whole and the true scatter is certainly greater. We also fit these data against log $(1 + z)$ by a simple linear regression as this measure of distance more closely follows look-back time. We find for the whole sample and by galaxy type:

$$q_{70} = 2.15 \pm 0.10 - 0.72 \pm 0.29 \times \log(1+z) \quad \text{(all)}, \tag{1}$$

$$q_{70} = 2.14 \pm 0.10 - 0.75 \pm 0.32 \times \log(1+z) \quad \text{(SFGs)}, \tag{2}$$

$$q_{70} = 2.31 \pm 0.21 - 1.59 \pm 0.52 \times \log(1+z) \quad \text{(AGN)}. \tag{3}$$

We observe a decrease in $q_{70}$ with redshift for the whole of the 70 μm detected sample which is principally due to sources with very high values of $q_{70}$ being found at low redshift, but which become much rarer at higher redshifts. This fit is shown in Fig. 2. The sample fitted here is naturally biased against low values of $q_{70}$ due to the 70 μm detection limit. We find that the SFGs show a similar trend to the total population, but although the AGN have a steeper slope they are almost consistent within the uncertainties and the slope is largely dependent on the lowest and highest redshift sources. All of these slopes are consistent with the decrease in observed $q_{70}$ seen in local templates redshifted to earlier epochs, e.g. as seen in Fig. 3.

### 3.3 Observed $q_{70}$ for the stacked sample

From our stacked images we obtained flux densities ranging between 0.3 and 2.5 mJy with uncertainties of ∼0.3 mJy. These flux densities correspond to 0.15 to 1.25 times the rms of the original image (2 mJy) showing a typical factor of ∼7 improvement in sensitivity. For each stacked measure of the 70 μm flux density, we calculate a mean value of $q_{70}$ by dividing by the mean radio flux density of the sources in a particular bin. In Fig. 3, we plot this value of $q_{70}$ as a function of redshift for both individual sources and stacks. In the four SFG redshift bins, we find significant detections of 70 μm flux density which give values of $q_{70}$ at the lower end of the distribution for SFGs. Hence, every SFG has a detection at 70 μm, either directly or indirectly. The stacked AGN are not detected in the lower ($z \leq 1$) redshift bin nor in the unknown redshift bin, but they are detected in the highest redshift bin ($1 \leq z \leq 5$). At each redshift, however, the stacked value of $q_{70}$ for AGN is at least 0.5 dex below that for SFGs.

### 3.4 Combined mean flux density ratio

In Fig. 3, we note that the whole population of radio-selected SFGs including non-detections at 70 μm has a scatter, i.e. range of values, in $q_{70}$ of at least one order of magnitude below $z = 1$. There is also a global trend towards lower values of $q_{70}$ at higher redshifts as seen with just the sources detected at 70 μm. The scatter for the AGN below $z = 1$ is larger, at least two orders of magnitude. The track of $q_{70}$ for a local *radio-loud* quasi-stellar object (QSO) (Elvis et al. 1994) remains very close to $q_{70} = -1$ for this whole redshift range (off the plot for the figures presented here). We note that typical values of $q_{70}$ for radio galaxies are $\geq -2$ using data from both low (Dicken et al. 2008) and high redshift samples (Seymour et al. 2007).

Given that we can detect all the SFGs at 70 μm, either individually or stacked, we can then examine the mean flux density ratio of the whole population as a function of redshift. We decrease the size of the redshift bin widths to half the prior value and make new stacked 70 μm images, but restrict our analysis to sources up to $z = 3$ as we have very few SFGs above this redshift. This decrease in bin size is important to provide fidelity in following any trend with redshift and is possible due to the larger number of sources per bin when including the detected and undetected sources. We combine the mean value of $q_{70}$ from the detected sources together with the stacked value of $q_{70}$ in these new bins by applying a weight scaled by the number of sources they represent in each bin. We derive the mean redshifts of each bin with a similar weighting scheme in log $(1 + z)$ space. The results of this approach are shown in Fig. 4 which demonstrates a steady decrease in the *observed* far-IR/radio ratio towards higher redshift. This decrease is steeper than that seen for the detected sources. We overlay the tracks of local SFGs from Rieke et al. (2009) at different luminosities ($\log [L_{\rm IR}/{\rm L}_{\odot}] = 10, 11, 12, 13$).

### 3.5 Selection issues

The work presented here, in particular Fig. 4, is naturally dependent on the initial separation of AGN and SFGs in S08 where a source was classified as an AGN by at least one of the methods discussed in the Introduction. While we are confident that the selection is correct in at least a statistical sense, it may fail on an individual basis as discussed in Section 4.1. Several of the discrimination methods in S08 (e.g. radio spectral index, radio morphology) were less effective for fainter sources, but this will change with upcoming data from surveys by e-MERLIN and Low Frequency ARay (LOFAR). Such data will be particularly important as SFGs are expected to dominate at fainter flux densities.

One possible bias in our selection of AGN in this work is the use of the 24 μm/radio flux density ratio as a diagnostic in S08. We used this flux density ratio ($q_{24}$) to select AGN as sources that were more than $5\,\sigma$ away from the lowest SFG track in $q_{24}$-redshift space. This selection could potentially lead to a bias against SFGs with low values of $q_{70}$. We identify 55/179 AGN solely on their value of $q_{24}$ (none of which were actually detected at 24 μm and hence are upper limits). When we repeated the whole analysis without the 24 μm/radio diagnostic, our mean values of $q_{70}$ for the SFGs in Figs 3 and 4 decreased by 0.03–0.1 dex. As this effect is small, we conclude the $q_{24}$ selection in S08 does not significantly affect the results presented here.

As discussed in Section 2.1, our initial radio survey is not complete at the faintest flux densities due to the effective decrease in survey area at the faintest levels. However, we have previously derived and used the necessary correction factors in S04. To asses whether their use here has any systematic effect, we reran our code without these correction factors and found very little difference to our results. In Figs 3 and 4, we observed a decrease in $q_{70}$ of ∼0.05 dex for the highest redshift bins with smaller differences at lower redshifts. Given the small size of this change and the successful use of these correction factors in previous publications, we believe any uncertainties in these correction factors do not significantly affect our results.

## 4 DISCUSSION

### 4.1 Direct detection of radio-selected AGN at 70 μm

An interesting result in Fig. 3 is the detection of eight radio-selected AGN at 70 μm. Given their redshifts, they have values of $q_{70}$ consistent with the SFG tracks. Hence, these sources are either AGN with unusually strong 70 μm emission or they are SFGs misidentified as AGN in S08.

Looking more closely at the reasons for their original selection as SFGs in S08, we see that four were selected due to their very flat or steep radio spectral index, three due to their compact radio morphology and one due to both its low radio/24 μm flux density ratio and its compact radio morphology. Of the sources selected by their spectral index, 2/4 have values that are close to the accepted range for SFGs. Given the low significance of these particular sources ($3–4\sigma$) at 4.8 GHz, their spectral index is more uncertain, hence it is possible that these sources may in fact be SFGs. The other two sources flagged by their spectral index have a very steep and a very flat spectrum well away from the range of SFGs. The four sources selected due to their radio morphology have compact unresolved radio emission from a 0.3 arcsec beam, but extended, elliptical optical morphology. The radio brightness temperatures of these sources are not high enough to definitely confirm an AGN origin to the radio emission and we cannot rule out the presence of compact nuclear starbursts.

It is also possible that some of these sources are hybrid AGN/SFG objects, i.e. they have a non-negligible contribution from star formation to the radio (in S08 we made the assumption that one process was completely dominant at radio wavelengths) or the

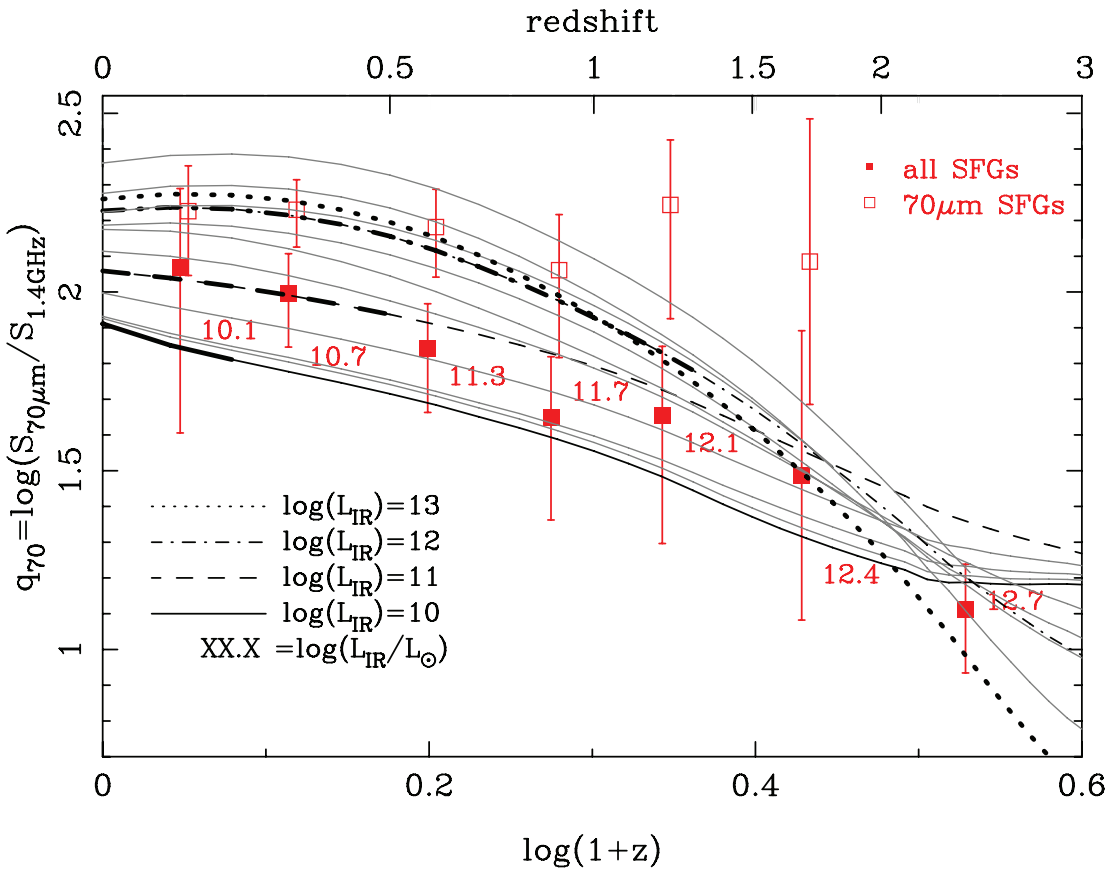


**Figure 4.** The mean value $q_{70}$ for all SFGs plotted as a function of redshift where we have combined the ratio for individual sources with the stacked value for undetected sources weighting them by the number of sources (filled red squares). Open red squares indicate the mean value of $q_{70}$ for our SFGs *detected* at 70 μm in the same redshift bins. Uncertainties are derived from measurement errors and Poisson statistics. The numbers beside each data point indicate the mean total IR luminosity (in units of log [$L_\odot$] and summed over 8–1000 μm) derived from the radio SFRs and the Kennicutt (1998) relation. The black lines again represent the tracks from local templates from Rieke et al. (2009) at luminosities indicted in the figure. These lines become thinner at the redshift, a given template becomes undetectable in our radio survey. The very thin grey lines represent tracks from templates at intermediate luminosities with intervals of 0.25 dex. The trend of a decrease in $q_{70}$ towards higher redshifts is generally consistent with tracks using local SEDs.

IR (e.g. Maiolino et al. 1995). For example, a radio source with 30 per cent of its radio flux density from star formation may still be selected as an AGN by some of the selection criteria in S08, but the value of $q_{70}$ for the star formation component would be just 0.5 dex higher than the hybrid value, still within the scatter for SFGs. Hence, simple flux density ratios, which currently are the dominant diagnostic at fainter flux densities, are not capable of diagnosing such hybrid objects. Given the short time-scale of the starburst and radio-loud AGN phase and the wide range of possible radio luminosities from both these processes, it is reasonable to expect the chances of detecting many hybrid sources in a blind radio survey to be low.

We note that only 8/92 sources detected at 70 μm are potential hybrids and that two maybe SFGs. Given the statistical approach of S08, to have a few potential misidentifications is not unexpected. If we were to assign all these sources as SFGs, our results in Fig. 4 would change by $\leq 0.02$ dex. The distribution of these 'hybrids' in the redshift/$q_{70}$ plane is only marginally different from the other detected sources (they have slightly lower values of $q_{70}$ at a given redshift). However, only two have uncertain radio AGN indicators, and the rest likely could be genuine AGN or hybrids as there is some evidence that Seyferts and radio-quiet AGN do follow the far-IR/radio correlation (Roy et al. 1998). This complication indicates the importance of future high-resolution and low-frequency radio data in determining the relative contribution of SFG and AGN within a single object as well as for a flux limited sample.

### 4.2 Decrease of observed $q_{70}$ at higher redshifts

In Fig. 4, we see that at $z = 0$ the $q_{70}$ values of the local empirical templates generally increase with total IR luminosity in the $10^{10-12}$ $L_\odot$ luminosity range. This increase is mainly due to the more luminous starbursts having SEDs which peak at shorter wavelengths, i.e. they may be characterized as having hotter dust. This trend is seen in empirical observations of local starbursts (Sanders & Mirabel 1996; Rieke et al. 2009). The exception is in the $10^{12-13}$ $L_\odot$ luminosity range where some of the intermediate tracks in grey have higher values of $q_{70}$ than the $10^{12}$ $L_\odot$ tracks while the $q_{70}$ for the $10^{13}$ $L_\odot$ track is very close to the $10^{12}$ $L_\odot$ track compared to these intermediate tracks. In this luminosity range, local sources show a relatively flat (i.e. $\alpha \geq -0.7$, where $S_\nu \propto \nu^\alpha$) radio spectrum at frequencies below 7 GHz which is attributed to free–free absorption and is reflected in the most luminous galaxy templates used here. While our mean values of $q_{70}$ for the SFGs follow the general decrease of the SED tracks towards higher redshifts, they mostly follow the LIRG (log [$L_{IR}/L_\odot$] $\geq 11$) track at low redshifts before moving to values in between the LIRG and 0.1× LIRG track across $0.5 \leq z \leq 1.5$. However, this redshift range is where the inferred

total IR luminosities from the radio or 70 μm flux densities are in the high-end LIRG and low-end ULIRG ($\log[L_{\rm IR}/{\rm L}_{\odot}] \sim 12$) regime. If our high-redshift LIRGs and ULIRGs had similar SEDs to their local counterparts, we would expect values of $q_{70}$ higher by ∼0.25 dex than we observe.

This discrepancy between the data and the appropriate SED track by luminosity is a maximum of $2\sigma$ in the $z \sim 0.86$ bin before the tracks begin to converge at higher redshifts. While we cannot completely rule out a few AGN contaminating our SFG sample, we calculate that we would need at least 30 per cent of the 52 SFGs in the $z \sim 0.86$ bin to be AGN with $q_{70} \sim 1$ to explain the observed difference.

This difference in observed and expected values of $q_{70}$ implies a change in the SED of $z \sim 1$ ULIRGs compared to local ones at moderate significance. For the ULIRGs, one possibility is that there is less free–free absorption at high redshift which would increase their radio flux density relative to the IR. This explanation could be true if star-forming regions in high-redshift ULIRGs are more extended (e.g. Chapman et al. 2004) and hence less optically thick than local ULIRGs. By extrapolating the rest frame ≥7 GHz unabsorbed radio power law to the lower frequencies probed by our 1.4 GHz observations, we can calculate the change in $q_{70}$ if no free–free absorption occurs in such objects. We find a decrease in the value of $q_{70}$ of 0.15(0.1) dex at $z = 0.5(1.5)$. This explanation could account for a considerable amount of the difference in $q_{70}$ for the most luminous sources.

Another possibility is that there is a change in the IR properties of LIRGs and ULIRGs at high redshift. There is evidence that a significant number of these sources at high redshift have different SEDs in comparison to local analogues, although the difference is not well determined and depends on selection (e.g. Rowan-Robinson et al. 2005; Papovich et al. 2007; Symeonidis et al. 2008). For example, Symeonidis et al. (2008) present evidence that many sources selected at 70 μm at $0.1 < z < 1.2$ have SEDs that are preferentially cold, while Papovich et al. (2007) find that the SEDs of bright 24 μm sources at $1.5 < z < 2.5$, on average, are preferentially warm. It is likely that the structure of the luminous star-forming regions are different in some ULIRGs at high redshift than locally, with more activity away from the compact nuclear sources that are typical for nearby ULIRGs (e.g. Chapman et al. 2004). This explanation would also permit the changes in radio emission discussed in the previous paragraph. The work presented here is unable to distinguish between a change in the IR SED, a change in the radio spectral index or even some combination of both. Determining the physical reasons for the differences between local and distant luminous starbursts will help us to understand the rapid change in SFR density from the present day to $z \sim 1$ where these high-luminosity objects dominate star-forming energy budget (Le Floc'h et al. 2005). Future observations by *Herschel* will be able to characterize these differences in detail.

### 4.3 Comparison with other studies

Many of the recent studies of the mid and far-IR/radio correlation (e.g. Boyle et al. 2007; Beswick et al. 2008; Garn & Alexander 2009) have examined values of $q_{\rm IR}$ as function of radio and/or IR flux density. Most IR/radio studies have been based on 24 μm data because of its higher sensitivity, but as we discussed in the Introduction, we use 70 μm data here as it more closely traces star formation. For our detected radio sources, we found a median value of $q_{70}$ comparable to that of Appleton et al. (2004), but we find evidence for a decrease towards higher redshifts unlike the non $k$-corrected data from Appleton et al. (2004). We used data from a narrower, but deeper survey in the radio and mid-IR which could explain why we see this decrease. In the only other study to use 70 μm data, Garn & Alexander (2009) examined the radio fluxes of 70 μm sources by stacking and found no evolution in $q_{70}$ over the 10–100 mJy 70 μm flux range (similar to the flux range of the 70 μm detected sources in this work).

Ibar et al. (2008) studied the 24 μm/radio correlation by examining the 24 μm properties of a sub-mJy radio sample. They found a decrease in observed (i.e. when no $k$-correction is applied) $q_{24}$ with redshift, but not as steep as that seen here with $q_{70}$. The shallower slope is likely due to the SED of the selected sources being flatter at the wavelengths seen by the 24 μm band. The 70 μm band used here probes longer wavelengths where the SED is rising more steeply in typical starbursts, hence the observed value of $q_{70}$ is likely to decrease more rapidly. Using an M82 $k$-correction those authors found an approximately constant value of $q_{24}$ up to $z \sim 3$. This value, $q_{24} = 0.71 \pm 0.47$, is lower than the value of $q_{70}$ observed here at any redshift. This difference can be explained by the shorter wavelengths probed by the 24 μm band which are well away from the peak of the IR luminosity that traces the bulk of the star formation. The value of $q_{24}$ also depends strongly on the SED assumed for the $k$-correction as Ibar et al. discuss and, furthermore, this value of $q_{24}$ is based on 24 μm detections only and makes no other discrimination between AGN and SFGs.

For a sample of 24 μm selected sources, Boyle et al. (2007) observed a systematically higher value of $q_{24}$ than seen by other authors. This value was constant with flux density. Given the selection wavelength and the lack of discrimination by galaxy type these authors are potentially selecting a large number of radio-quiet AGN which have strong observed 24 μm emission, but relatively little radio emission. However, in a similar study of 24 μm selected sources Beswick et al. (2008) found that the observed value of $q_{24}$ decreased towards fainter 24 μm flux densities and also decreased slightly towards higher redshifts. In fact, at the faintest flux densities, the Beswick et al. (2008) result was almost an order of magnitude lower than that seen by Boyle et al. (2007). This discrepancy has not been fully explained although it is possible that the difference is a result of the different radio telescopes and the different resolutions used (Australian Telescope Compact Array (ATCA) and MERLIN for Boyle et al. and Beswick et al., respectively).

### 4.4 Comparison with models of the far-IR/radio relation

While the ultimate origin of the far-IR/radio correlation is hot, young stars in dusty regions of the galaxy, the origin of the radiation we observe is not completely cospatial or cotemporal. The wavelength range of far-IR radiation probed by original *IRAS* 60 and 100 μm band (and MIPS 70 μm band used here) originates from dust clouds relatively close to the young stars and emits fairly promptly after a localized burst of star formation whereas radio emission originates from electrons travelling through the galaxy and interacting with its magnetic field which can happen relatively far and later than the original formation of stars. This difference in origin of the two wavelengths explains the scatter we do see in the local relation (Yun et al. 2001) and the scatter within galaxies (Murphy et al. 2006). However, this difference also suggests that there is a dependence of the far-IR/radio correlation with the nature and mode of the very recent and instantaneous star formation.

Bressan et al. (2002) have performed detailed modelling of the far-IR/radio correlation using the concept of age-selective obscuration (i.e. where younger stars and their corresponding emission

lie in denser molecular clouds) to derive SEDs and potential observables for a range of galaxy ages and SFRs. They find that the luminosity (far-IR or radio) to SFR ratio does vary by up to an order of magnitude with the age of the starburst for a range of star formation histories. Although these variations partly cancel out, these authors do predict a variation of $q_{\rm IR}$ with starburst age which appears stronger for starbursts with shorter e-folding times. They postulate that a low value of $q_{\rm IR}$ could be simply the natural consequence of a particular, e.g. post-starburst, phase in a galaxy's history. Hence, a further possible explanation for our low value of $q_{70}$ could simply be the phase the starburst is in. Bressan et al. (2002) do predict an evolutionary path through the $q_{\rm IR}$/radio spectral index parameter space which could be used to determine the age of the starburst should sufficiently accurate IR and radio data be available in the future.

## 5 CONCLUSIONS

For the first time, the far-IR/radio correlation of radio-selected SFGs and AGN has been examined to high redshifts for a large number of sources. The 70 μm band is a more direct tracer of the bulk of the IR luminosity than 24 μm and avoids many complicated spectral features in the mid-IR. Throughout this paper, we adopted a philosophy of studying *observed* flux density ratios as a function of redshift and comparing to the ratio observed from a redshifted SED rather than apply a *k*-correction. This approach avoids the problem of choosing which template to use in making a *k*-correction which can be problematic given the range of SEDs used previously for similar work, e.g. M82 and Arp220, and their application at high redshift.

We have shown that:

(i) Due to current radio and far-IR survey limits, only sources with relatively high values of observed $q_{70}$ are detected at 70 μm.

(ii) The radio sources detected at 70 μm have similar observed median values and uncertainties in $q_{70}$ as reported previously by a similarly selected sample (Appleton et al. 2004), but also show evidence of a systematic decrease towards high redshift despite the bias towards high values of $q_{70}$ due to the 70 μm detection limit of the currently available data.

(iii) Of those radio sources detected at 70 μm, 84/92 were previously identified as radio-selected SFGs. On closer examination due to their detection at 70 μm, two of the remaining eight sources, identified as radio-selected AGN in S08, are thought to be SFGs, or to show a significant contribution from star formation, due to uncertainty in their radio spectra.

(iv) When stacking the sources not detected at 70 μm by galaxy type and redshift, we find a stacked detection in each of the four redshift bins for the SFGs, but only detect the AGN in the highest redshift bin. In the lower redshift and unknown redshift AGN bins, we do not find a stacked detection down to ∼0.3 mJy. The SFGs have stacked flux densities not much below our original 70 μm detection limit, hence the inferred values of $q_{70}$ are only slightly below those seen for the individually detected SFGs.

(v) In order to examine the far-IR/radio correlation, we determined the value of $q_{70}$ for all the radio selected SFGs. The mean values of $q_{70}$ for the detected and non-detected radio-selected SFGs were combined with appropriate weighting and we find an observed value of $q_{70}$ that decreases towards higher redshift as expected from tracks derived from empirical SEDs of local SFGs.

(vi) When the observed values of $q_{70}$ for the SFGs are compared closely to tracks of local SEDs at the appropriate luminosity/SFR, we find that while they broadly agree at low redshift the observed $q_{70}$ at $z \sim 1$ (for sources close to ULIRG luminosities) is $2\sigma$ below the value seen for local ULIRGs shifted to this redshift. This result implies a difference in the SED of local and $z \sim 1$ ULIRGs, and demonstrates the value of future comparisons using bolometric luminosities when examining the far-IR/radio correlation at high redshift. At redshifts higher than $z \sim 1$, the tracks of local SFGs converge and our observed values of $q_{70}$ have higher uncertainties, hence we are unable to determine whether such a difference persists to higher redshifts from this data set.

We cannot completely rule out that part of this last result is due to AGN contaminants, although it would require a large fraction of radio-excess sources. The lower value $q_{70}$, beyond that simply inferred by the shifting of the band pass with redshift is consistent with other results in the literature that suggest that LIRGs and ULIRGs at high redshift are a more diverse population than their local counterparts (Rowan-Robinson et al. 2005; Sajina et al. 2006; Brand et al. 2008; Symeonidis et al. 2008). The full range of ULIRG properties at high redshift will be revealed by *Herschel* which will be the first telescope to truly select such objects based on their directly observed bolometric luminosities.

## ACKNOWLEDGMENTS

We thank the anonymous reviewer for many helpful comments that improved the clarity and presentation of this paper. This work is based in part on observations made with the *Spitzer Space Telescope*, which is operated by the Jet Propulsion Laboratory, California Institute of Technology under a contract with NASA. Support for this work was provided by NASA through an award issued by JPL/Caltech. The National Radio Astronomy Observatory is a facility of the National Science Foundation operated under cooperative agreement by Associated Universities, Inc. This work was partially supported by JPL/Caltech contract 1255094 to the University of Arizona.

## REFERENCES

Appleton P. N., Marleau F. et al., 2004, ApJS, 154, 147
Beers T. C., Flynn K., Gebhardt K., 1990, AJ, 100, 32
Bell E. F., 2003, ApJ, 586, 794
Beswick R. J., Muxlow T. W. B., Thrall H., Richards A. M. S., Garrington S. T., 2008, MNRAS, 385, 1143
Boyle B. J., Cornwell T. J., Middelberg E., Norris R. P., Appleton P. N., Smail I., 2007, MNRAS, 376, 1182
Brand K. et al., 2008, ApJ, 673, 119
Bressan A., Silva L., Granato G. L., 2002, A&A, 392, 377
Chapman S. C., Smail I., Windhorst R., Muxlow T., Ivison R. J., 2004, ApJ, 611, 732
Condon J. J., 1992, ARA&A, 30, 575
Condon J. J., Huang Z.-P., Yin Q. F., Thuan T. X., 1991, ApJ, 378, 65
Dicken D., Tadhunter C., Morganti R., Buchanan C., Oosterloo T., Axon D., 2008, ApJ, 678, 712
Donley J. L., Rieke G. H., Rigby J. R., Pérez-González P. G., 2005, ApJ, 634, 169
Elvis M. et al., 1994, ApJS, 95, 1
Frayer D. T. et al., 2006, ApJ, 647, L9
Garn T., Alexander P., 2009, MNRAS, 394, 105
Garrett M. A., 2002, A&A, 384, L19
Helou G., Soifer B. T., Rowan-Robinson M., 1985, ApJ, 298, L7
Hopkins A. M., 2004, ApJ, 615, 209
Hughes A., Wong T., Ekers R., Staveley-Smith L., Filipovic M., Maddison S., Fukui Y., Mizuno N., 2006, MNRAS, 370, 363

Huynh M. T., Frayer D. T., Mobasher B., Dickinson M., Chary R.-R., Morrison G., 2007, ApJ, 667, L9
Ibar E. et al., 2008, MNRAS, 386, 953
Kennicutt R. C., 1998, Ann. Rev. Astron. Astrophys., 36, 189
Kovács A., Chapman S. C., Dowell C. D., Blain A. W., Ivison R. J., Smail I., Phillips T. G., 2006, ApJ, 650, 592
Le Floc'h E. et al., 2005, ApJ, 632, 169
Maiolino R., Ruiz M., Rieke G. H., Keller L. D., 1995, ApJ, 446, 561
Miller N. A., Owen F. N., 2001, AJ, 121, 1903
M$^{c}$Hardy I. M. et al., 1998, Astron. Nachr., 319, 51
Murphy E. J. et al., 2006, ApJ, 651, L111
Papovich C. et al., 2007, ApJ, 668, 45
Rieke G. H. et al., 2004, A&AS, 154, 25
Rieke G. H., Alonso-Herrero A., Weiner B. J., Pérez-González P. G., Blaylock M., Donley J. L., Marcillac D., 2009, ApJ, 692, 556
Rowan-Robinson M., Broadhurst T. J., Lawrence A., McMahon R. G., Lonsdale C. J., 1991, Nat, 351, 719
Rowan-Robinson M. et al., 2005, AJ, 129, 1183
Roy A. L., Norris R. P., Kesteven M. J., Troup E. R., Reynolds J. E., 1998, MNRAS, 301, 1019
Sajina A., Scott D., Dennefeld M., Dole H., Lacy M., Lagache G., 2006, MNRAS, 369, 939
Sanders D. B., Mirabel I. F., 1996, ARA&A, 34, 749
Seymour N., McHardy I. M., Gunn K. F., 2004, MNRAS, 352, 131 (S04)
Seymour N. et al., 2007, ApJS, 171, 353
Seymour N. et al., 2008, MNRAS, 386, 1695 (S08)
Spergel D. et al., 2003, A&AS, 148, 175
Symeonidis M., Willner S. P., Rigopoulou D., Huang J.-S., Fazio G. G., Jarvis M. J., 2008, MNRAS, 385, 1015
Vlahakis C., Eales S., Dunne L., 2007, MNRAS, p. 605
Werner M. W. et al., 2004, A&AS, 154, 1
Yun M. S., Reddy N. A., Condon J. J., 2001, ApJ, 554, 803

This paper has been typeset from a TEX/LATEX file prepared by the author.